Materials Advances

ROYAL SOCIETY OF CHEMISTRY

PAPER

View Article Online
View Journal | View Issue

Cite this: *Mater. Adv.*, 2025, 6, 4513

Gold recovery from acidic wastewater using ionic viologen organic and metal–organic framework composites†

Sk Abdul Wahed, Atikur Hassan * and Neeladri Das *

Received 2nd April 2025,
Accepted 28th May 2025

DOI: 10.1039/d5ma00306g

rsc.li/materials-advances

This study reports syntheses of a set of unique ionic hybrid composites to efficiently remove gold anions from acidic wastewater. The hybrid composites were easily obtained using a well-known metal–organic framework (MOF) and an ionic viologen organic framework (iVOF) that were thoroughly characterized. The highest uptake capacity recorded by iVOF-2@MOF_Comp-3 was 1053 mg g^{-1} within three hours. This adsorbent was also able to quantitatively (>99%) remove gold species within fifteen minutes from a highly acidic (pH = 1) aqueous solution with a distribution coefficient (K_d) greater than 10^5 mL g^{-1}. The hybrid composite adsorbent could also be recycled easily, thus fulfilling most of the criteria expected in effective adsorbents.

1. Introduction

Gold is indispensable in jewellery, catalysis and electronics due to its remarkable properties, including excellent conductivity, corrosion resistance and a high melting point.[1–3] As such, presence of gold species is well-known in electronic waste (e-waste).[4,5] More efficient production and recycling techniques are essential as gold is a valuable but finite resource.[6] Traditional pyro-metallurgical processes are polluting, energy intensive and inefficient. Due to the fact that e-waste contains 10–100 times higher concentrations of gold than natural ores, the recovery of gold from e-waste is becoming increasingly important. Moreover, the quantum of e-waste is increasing and an efficient recycling infrastructure is needed.[7,8] Adsorption, chemical precipitation, ion exchange and solvent extraction are some of the current recovery techniques, but their high energy consumption and inefficiencies limit their effectiveness.[9–13]

Metal–organic frameworks (MOFs) are porous materials with diverse and desirable properties (chemical and physical).[14] Consequently, MOFs have been studied for a wide range of applications, including effective trapping of small molecules/ions and separating mixtures based on steric, stereochemical, and reactivity properties.[15,16] However, a significant drawback of MOF-based adsorbents is their slow sorption rate.[17,18] On the other hand, adsorbents based on ionic viologen-based organic frameworks (iVOFs) demonstrate relatively much faster sorption kinetics towards anionic pollutants relative to MOFs.[19,20] It is proposed that the hybrid composite material, obtained from MOFs and iVOFs, would be a better adsorbent with superior performance.[20] Furthermore, the hybrid composite is anticipated to demonstrate improved efficiency and effectiveness in gold recovery processes. To date, no ionic hybrid composite has shown rapid and selective extraction of gold from a solution containing other complex ions. This gap (in gold extraction/recovery) has led us to explore using MOF-iVOF composites to extract Au species from diverse gold-containing wastewater sources. Herein, we report the syntheses of novel ionic MOF-polymer hybrid composites that were explored as adsorbents to remove gold species from aqueous solutions at various pH. The maximum uptake capacity and kinetics associated with trapping of gold species were studied, and their performance was compared to that of previously reported adsorbents for this application.

2. Results and discussion

This study focuses on developing strategic composite materials decorated with useful functional groups that would assist in improving the role of the material as an adsorbent. Specifically, we have synthesized MOF-iVOF composites (Scheme 1) specially tailored for removing gold species from acidic aqueous solutions. Firstly, MOF UiO-66-NH_2 was synthesized following a previously reported synthetic protocol (details in the Experimental section).[21] Next, the pristine ionic viologen organic framework (iVOF-2) was prepared using the Sonogashira cross-

Department of Chemistry, Indian Institute of Technology Patna, Patna 801106, Bihar, India. E-mail: atikurhassan@gmail.com, neeladri@iitp.ac.in, neeladri2002@yahoo.co.in

† Electronic supplementary information (ESI) available: Characterization of the compounds, capture studies, and comparison tables. See DOI: https://doi.org/10.1039/d5ma00306g

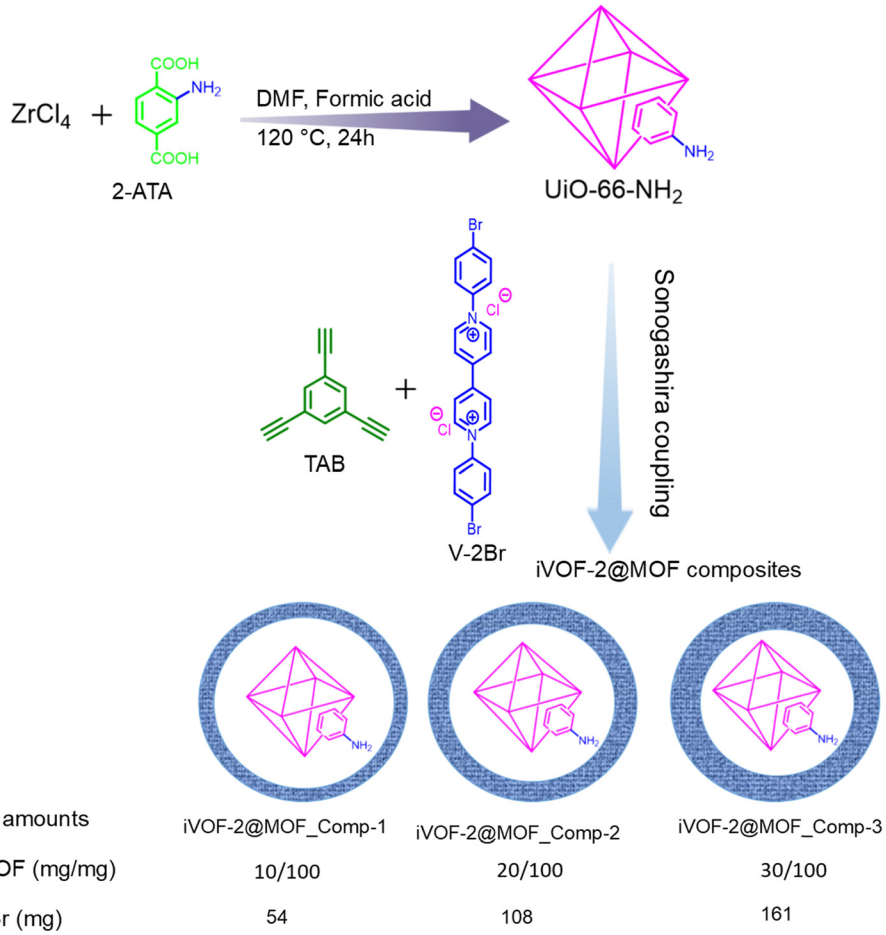

Scheme 1 Design of the synthesis of ionic iVOF-2@MOF composites.

coupling reaction (details in the Experimental section). Upon successful synthesis of the MOF (UiO-66-NH_2) and iVOF-2, attempts were made to obtain the composite material using the one-pot core–shell methodology by varying the amount of the precursor monomers for making iVOF-2 (details in the Experimental section). While synthesizing the composite, different compositions of iVOF-2 precursors (TAB and V-2Br monomers in Scheme 1) were added in an inert environment to a toluene suspension of the pristine MOF (UiO-66-NH_2) in the presence of other reagents required in Sonogashira coupling reaction. Upon completion of the reaction, the precipitated products were obtained *via* centrifugation. The isolated solids were subsequently washed thoroughly with methanol, DCM, acetonitrile, THF, and acetone and finally dried in an oven to get three hybrid composites, namely iVOF-2@MOF_Comp-1, iVOF-2@MOF_Comp-2 and iVOF-2@MOF_Comp-3.

Pristine samples of UiO-66-NH_2, iVOF-2, and their composites were thoroughly characterized using powder X-ray diffraction (P-XRD), Fourier transform infrared (FT-IR) spectroscopy, solid-state ^{13}C nuclear magnetic resonance spectroscopy (^{13}C CP-MAS), low-temperature N_2 sorption analysis, X-ray photoelectron spectroscopy (XPS), field emission scanning electron microscopy (FE-SEM) and energy dispersive X-ray (EDX) analysis.

The P-XRD analysis of the MOF UiO-66-NH_2 reveals its highly crystalline nature, while iVOF-2 is amorphous. Furthermore, the PXRD pattern of the synthesized MOF was compared with that corresponding to the simulated pattern of UiO-66-NH_2 (Fig. S1, ESI†), and the PXRD pattern confirmed the successful synthesis of UiO-66-NH_2. Interestingly, the composite materials (iVOF-2@MOF_Comp-1 to 3) exhibit crystallinity, which confirms the presence of UiO-66-NH_2 in the matrices of the composites (Fig. 1a). The FT-IR spectra of the composites, along with UiO-66-NH_2 and iVOF-2 (Fig. S2, ESI†), also confirmed the presence of both components (UiO-66-NH_2 and iVOF-2) in the matrices of the resultant composite. Additionally, solid-state ^{13}C CP-MAS NMR spectra (Fig. 1b) provided structural insights with the appearance of two distinct peaks at around ~170 ppm (attributed to unsymmetrical carboxylic –C═O– carbon atoms) and at ~150 ppm (due to the carbon atoms linked to amine groups).

Porosity analysis using low-temperature N_2 sorption data (Fig. 1c and Fig. S3, ESI†) of UiO-66-NH_2 confirms its highly porous nature and higher surface area (1331 $m^2\ g^{-1}$) compared to that of iVOF-2 (158 $m^2\ g^{-1}$). The surface area of the composites iVOF-2@MOF_Comp-1 to 3 are 742, 628, and 466 $m^2\ g^{-1}$, respectively. Overall, the surface area decreased in the following order: UiO-66-NH_2 > iVOF-2@MOF_Comp-1 > iVOF-2@MOF_Comp-2 >

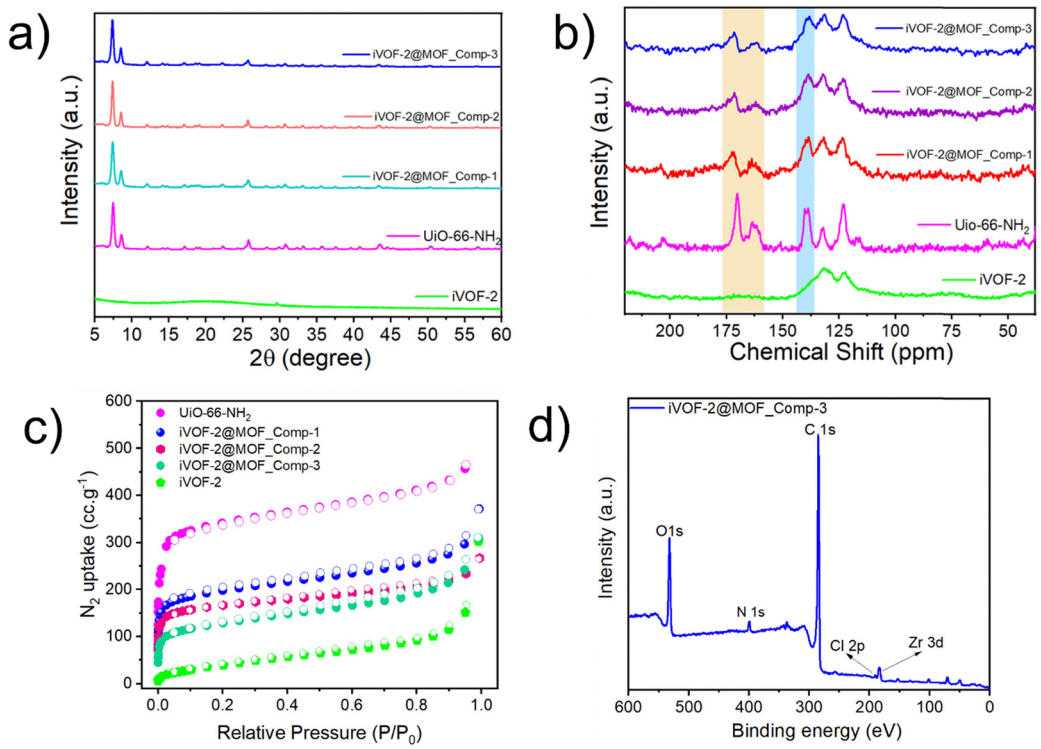

Fig. 1 (a) PXRD patterns of the UiO-66-NH_2, iVOF-2 and iVOF-2@MOF_Comp-1 to 3, (b) solid state ^{13}C NMR of the UiO-66-NH_2, iVOF-2 and the iVOF-2@MOF_Comp-1 to 3, (c) low temperature N_2 sorption isotherms of UiO-66-NH_2, iVOF-2 and the iVOF-2@MOF_Comp-1 to 3 and (d) XPS survey spectrum of iVOF-2@MOF_Comp-3.

iVOF-2@MOF_Comp-3 > iVOF-2. The pore size distribution (PSD) analysis indicates that the pristine MOF is predominantly microporous in nature, whereas the iVOF-2 composites exhibit mesoporous characteristics (Fig. S3, ESI†). Notably, the degree of mesoporosity increases with the amount of polymer incorporated into the composite material. This trend suggests that Comp-3, which contains the highest polymer content among the three composites (iVOF-2@MOF_Comp-1, iVOF-2@MOF_-Comp-2, and iVOF-2@MOF_Comp-3), displays the most pronounced mesoporosity (Fig. S3, ESI†). This evolution in pore structure highlights the role of polymer integration in tuning the textural properties of the composite materials.

The difference in the magnitude of the surface area of the composites concerning that of the precursors (UiO-66-NH_2 and iVOF-2) also ratified the presence of both MOF and iVOF-2 in them. The XPS analysis of the iVOF-2@MOF_Comp-3 indicates the presence of C, N, O, Zr, and Cl in the XPS survey spectra (Fig. 1d). Also in the HR-XPS of iVOF-2@MOF_Comp-3 the binding energies for C 1s, N 1s, and Zr 3d were observed indicating the formation of the composite materials (Fig. S4, ESI†). The morphology of the iVOF-2, UiO-66-NH_2 and iVOF-2@MOF_Comp-3 was studied by capturing FE-SEM images (Fig. 2a, b and Fig. S5, S7, S9, ESI†). Further insights into the composition of iVOF-2, UiO-66-NH_2, and iVOF-2@MOF_Comp-3 were obtained from EDX and mapping analysis data (Fig. 2c and Fig. S6, S8, S10, ESI†). The EDX spectrum of iVOF-2 exhibited the presence of only C, N, and Cl, while that of UiO-66-NH_2 showed the presence of C, N, Zr, and O. As expected, the EDX spectrum of the composites showed the presence of C, N, O, Zr, and Cl. Thus, mapping analyses provided further evidence to support the formation of the composites.

From the characterization data, it may be concluded that the composites (iVOF-2@MOF_Comp-1 to 3) reported herein feature (i) moderately high surface areas, (ii) a polymeric backbone with ample ion exchange sites, and (c) secondary binding units of UiO-66-NH_2 (Zr-secondary binding units: Zr-SBUs). Previous reports indicate that UiO-66-NH_2 can capture $AuCl_4^-$ *via* binding the anions with Zr-SBUs.[9] Also, there are reports wherein ionic POPs were explored as adsorbent materials for capturing $AuCl_4^-$ *via* an ion-exchange-based mechanism.[22,23] However, UiO-66-NH_2 and ionic porous adsorbents are individually associated with limitations such as slow uptake kinetics, low uptake capacity, or physiochemical instability. In this context, we envisioned that the composites reported herein may overcome the problems recorded for either MOFs or iVOFs. The presence of ion exchange sites and secondary binding units (Zr-SBU) in the porous composites with moderate surface areas (450–750 $m^2\ g^{-1}$) motivated us to explore their abilities to capture gold ($AuCl_4^-$) species from acidic waste. The $AuCl_4^-$ removal efficiencies recorded for iVOF-2, UiO-66-NH_2, and their composites (iVOF-2@MOF_Comp-1 to 3) are shown in Fig. 3a (detail capture experiments in the ESI†).

The results indicate that iVOF-2@MOF_Comp-3 exhibited the highest removal efficacy, followed by iVOF-2@MOF_Comp-2, iVOF-2@MOF_Comp-1, iVOF-2, and finally UiO-66-NH_2. Notably,

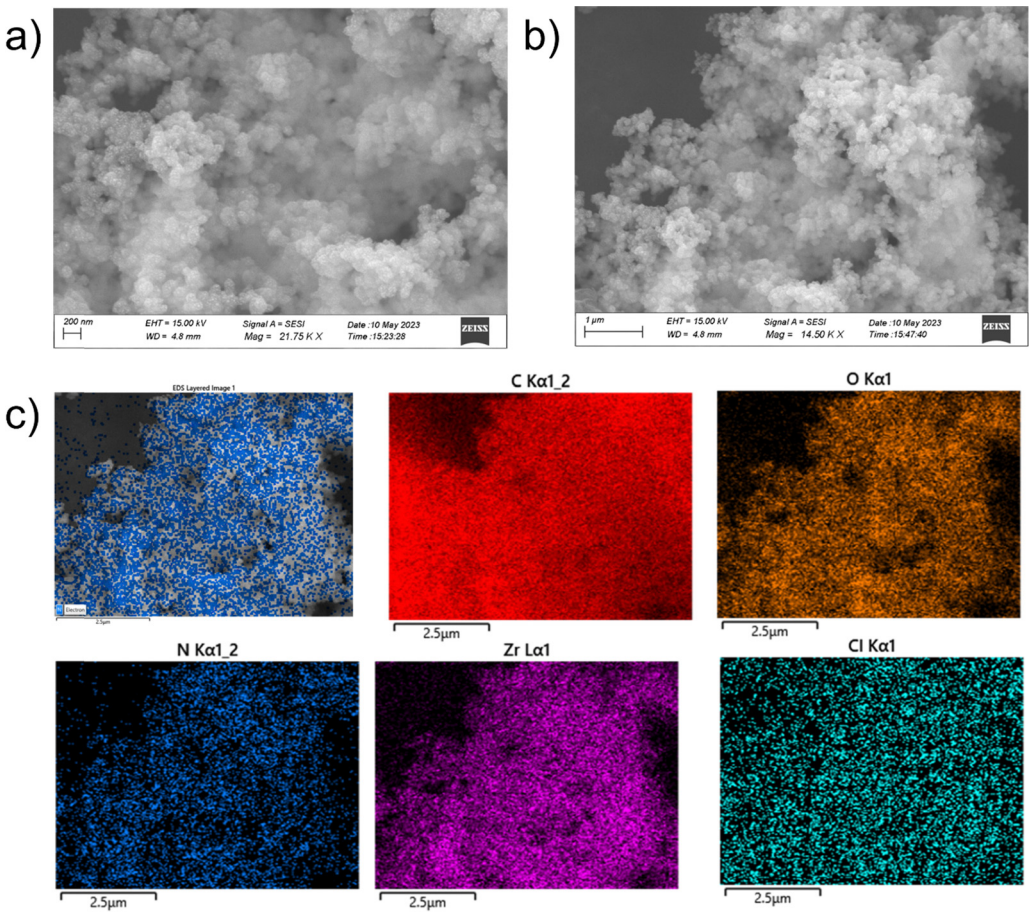

Fig. 2 (a) and (b) FESEM images of iVOF-2@MOF_Comp-3 at different magnifications and (c) EDX mapping of the iVOF-2@MOF_Comp-3 indicates the presence of C, N, O, Zr and Cl.

iVOF-2@MOF_Comp-3 demonstrated a remarkable removal efficiency of 99.99%. Subsequently, time-dependent studies were conducted using samples of iVOF-2, UiO-66-NH_2, and iVOF-2@MOF_Comp-3 (Fig. 3b). The experimental results show that the capture of $AuCl_4^-$ by iVOF-2@MOF_Comp-3 is much faster than that for iVOF-2 and UiO-66-NH_2. The kinetic data fitted well to a pseudo-second-order model with a high correlation coefficient (>0.99) (Fig. 3c). Furthermore, the maximum capture capacity of these materials was determined using the Langmuir adsorption isotherm model (Fig. S11–S13, ESI†). iVOF-2@MOF_Comp-3 exhibited the highest uptake capacity (1053 mg g^{-1}), which was much higher than that of both precursors, *i.e.*, pristine samples of MOF (645.00 mg g^{-1}) and iVOF-2 (826 mg g^{-1}) [detail in comparison Tables S1 and S2, ESI†]. Notably, most gold capture studies reported in the literature were conducted under less acidic conditions (*e.g.*, UiO-66-MTD at pH 5, Pc–POSS–POPs at pH 5, and AN-POP at pH 5), whereas our capture experiments were performed under more acidic conditions (pH 1), demonstrating the robustness of our material under harsh environments.[24,25] Furthermore, the gold capture capacity of our material iVOF-2@MOF_Comp-3, is among the highest reported to date, outperforming several benchmark materials such as TTASDFP (245 mg g^{-1}), Pc–POSS–POPs (862.07 mg g^{-1}), Fe-BTC/PpPDA (934 mg g^{-1}), UiO-66-BTU (680.20 mg g^{-1}), and V-PPOP-Br (792.22 mg g^{-1}) [detail in comparison Table S1, ESI†].[3,22,24,26–28] In addition, iVOF-2@MOF_Comp-3 exhibits significantly faster gold ion removal kinetics compared to previously reported materials such as PAF-1, COF-Tp-Tsc, and PCS-ST [detail in comparison Table S2, ESI†].[29–31] To assess the effects of other anions on the gold removal efficiency of iVOF-2@MOF_Comp-3, its removal efficiency was tested in the presence of various anions. Fig. 3d illustrates the negligible effects of anions on the removal of $AuCl_4^-$ by the composite sample, indicating that the presence of a variety of different anionic species has a minimal or insignificant impact on its gold species removal efficiency. Moreover, gold scavenging efficiencies of iVOF-2@MOF_Comp-3 were also conducted using water samples collected from various sources (Fig. S14, ESI†). Remarkably, iVOF-2@MOF_Comp-3 consistently removed over 95% of gold species in all tested conditions, with the K_d value exceeding 10^5 mL g^{-1}. These findings suggest that iVOF-2@MOF_Comp-3 is a strategic adsorbent material for capturing gold from diverse aqueous media. The pH of a solution significantly influences the adsorption behavior of metal ions. In this study, we explored how pH effects the adsorption of Au(III) by adjusting the pH of the solution from 1 to 7 using NaOH and HCl. As shown in Fig. S15 (ESI†), a high removal efficiency of iVOF-2@MOF_Comp-3 was observed in the pH range of 1 to 7.

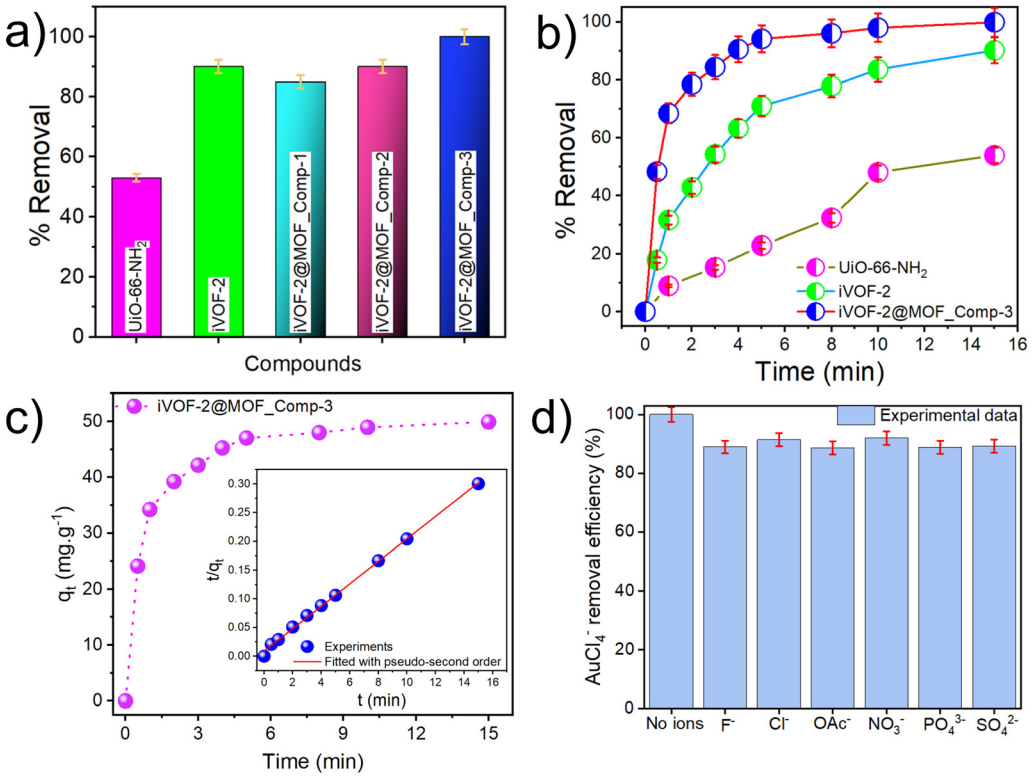

Fig. 3 (a) Removal of $AuCl_4^-$ by UiO-66-NH_2, iVOF-2 and iVOF-2@MOF_Comp-1 to 3, (b) time dependent removal of $AuCl_4^-$ by UiO-66-NH_2, iVOF-2 and iVOF-2@MOF_Comp-3, (c) pseudo second order uptake curve for iVOF-2@MOF_Comp-3 and (d) effects of other anions during removal of $AuCl_4^-$ by iVOF-2@MOF_Comp-3.

To gain further insight into the mechanism of gold capture by iVOF-2@MOF_Comp-3, its gold-loaded samples (Au@iVOF-2@MOF_Comp-3) were analyzed using various techniques. Powder X-ray diffraction (PXRD) analysis is invaluable for identifying the presence of gold in loaded samples. For reference, the PXRD pattern of pure 24 carat gold was recorded, revealing characteristic peaks corresponding to the planes 111, 200, 220, and 311, which can be assigned to the diffraction of metallic gold. As expected, some of these same peaks were also observed in the samples of Au@iVOF-2@MOF_Comp-3 (Fig. 4a).

Conversely, pristine samples of iVOF-2@MOF_Comp-3 did not exhibit any diffraction peaks matching these planes. This confirmed the presence of gold species in Au@iVOF-2@MOF_Comp-3. This insightful information was also verified by XPS analysis (Fig. S16 and S17, ESI†). In the XPS survey spectrum of the Au@iVOF-2@MOF_Comp-3, the presence of Au along with other elements indicates tapping of gold by the composite (Fig. S16, ESI†). Furthermore, during the ion exchange process of the $AuCl_4^-$ ions, these are also co-ordinated with SBU of the UiO-66-NH_2, having electrostatic interactions with the protonated amino groups during the adsorption process. XPS analysis indicates the presence of Au 4f 5/2 and 7/2 in the XPS spectrum with a binding energy in the range of 82 to 90 eV (Fig. 4b).[4,10,32] The fitted peaks at 89.97 and 86.14 are due to Au(III), whereas those at 88.33 and 84.75 eV are due to Au(0).[29,33] Energy-dispersive X-ray spectroscopy (EDS) and elemental mapping analysis indicated a homogeneous distribution of gold species alongside other elements (Fig. 4c and Fig. S18, S19, ESI†). Thus, EDS analysis provided further evidence of the presence of gold in Au@iVOF-2@MOF_Comp-3. Furthermore, significant changes in FT-IR spectra, after exposure of samples of iVOF-2@MOF_Comp-3 to $AuCl_4^-$ (aq), also provided evidence of the presence of favorable interactions between gold species and the MOF-iVOF composites reported herein (Fig. S20, ESI†). Overall, these experimental data may be considered cumulative evidence that strongly supports the successful capture of gold by the composites. Furthermore, the reusability tests showed that the composites could be reused for up to three cycles with no significant decrease in gold ($AuCl_4^-$) removal efficiency (Fig. 5a). Finally, we also characterized the reused iVOF-2@MOF_Comp-3 with FTIR, P-XRD and porosity analysis (Fig. 5b–d). It can be seen that after several cycles of capture, the iVOF-2@MOF_Comp-3 was identical when compared with the pristine iVOF-2@MOF_Comp-3. This highlights the robustness and practical applicability of the iVOF-2@MOF composites for repeated use in gold capture applications in an economically viable manner.

3. Conclusions

This study presents a facile method for the synthesis of ionic MOF_iVOF composites without post-modification, which offers a clear advantage over other ionic composites. Among the three composites, iVOF-2@MOF_Comp-3 emerges as the most effective, showing rapid and efficient capture of gold species from acidic

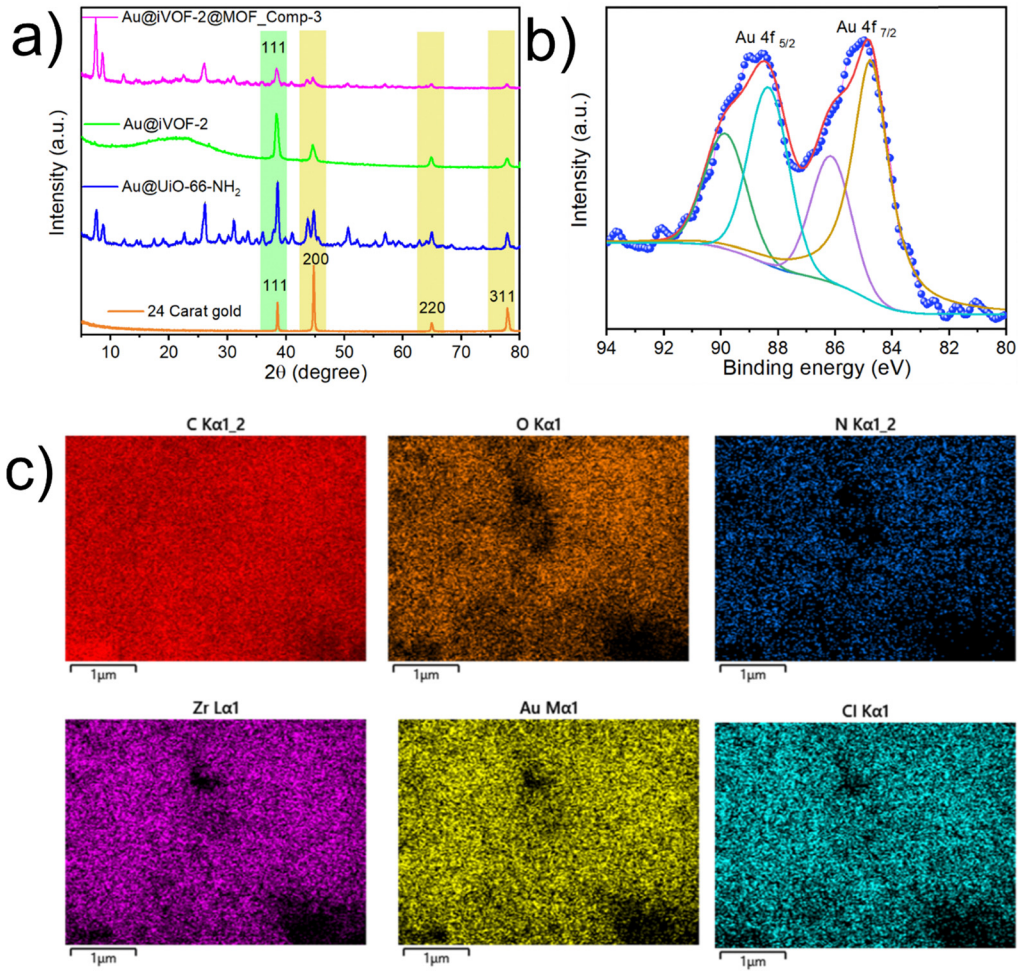

Fig. 4 (a) PXRD patterns of 24 karat gold, Au@UiO-66-NH_2, Au@iVOF-2 and the Au@iVOF-2@MOF_Comp-3, (b) XPS analysis of Au in Au@iVOF-2@MOF_Comp-3 and (c) elemental mapping of the Au@iVOF-2@MOF_Comp-3.

solutions with a high partition coefficient ($K_d > 10^5$ mL g^{-1}). Furthermore, it performs well in real water samples, even in the presence of co-existing ionic contaminants. The method holds promise for the development of other MOF_iVOF composites, particularly for the recovery of precious metals from industrial waste, making it a valuable approach to sustainable resource recovery.

4. Experimental section

4.1. Synthesis of the MOF (UiO-66-NH_2)

UiO-66-NH_2 was synthesized following a literature procedure.[21] In a 20 mL vial, 2-amino-terephthalic acid (2-ATA) (0.13 g, 0.72 mmol), zirconium(IV) chloride (0.17 g, 0.72 mmol), and formic acid (0.8 mL) were dissolved in DMF (8 mL). The vial was then sealed with Teflon tape and a cap, and the reaction mixture was heated at 120 °C for 24 hours. During this time, a white powder gradually formed. The powder was collected by centrifugation, washed with methanol, and dried under vacuum.

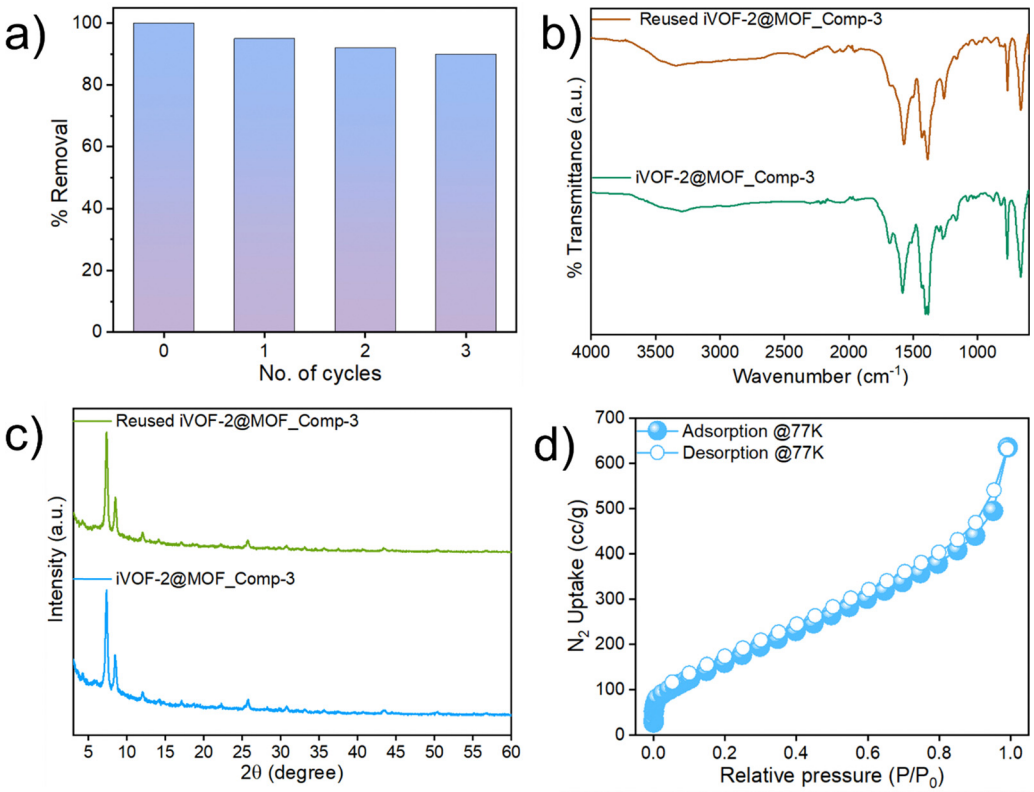

Fig. 5 Recyclability of the iVOF-2@MOF_Comp-3 for gold capture, (b) FT-IR of the pristine iVOF-2@MOF_Comp-3 and reused iVOF-2@MOF_Comp-3, (c) PXRD of the pristine iVOF-2@MOF_Comp-3 and reused iVOF-2@MOF_Comp-3 and (d) N_2 sorption analysis of the reused iVOF-2@MOF_Comp-3.

4.2. Synthesis of the V-2Br[34–36]

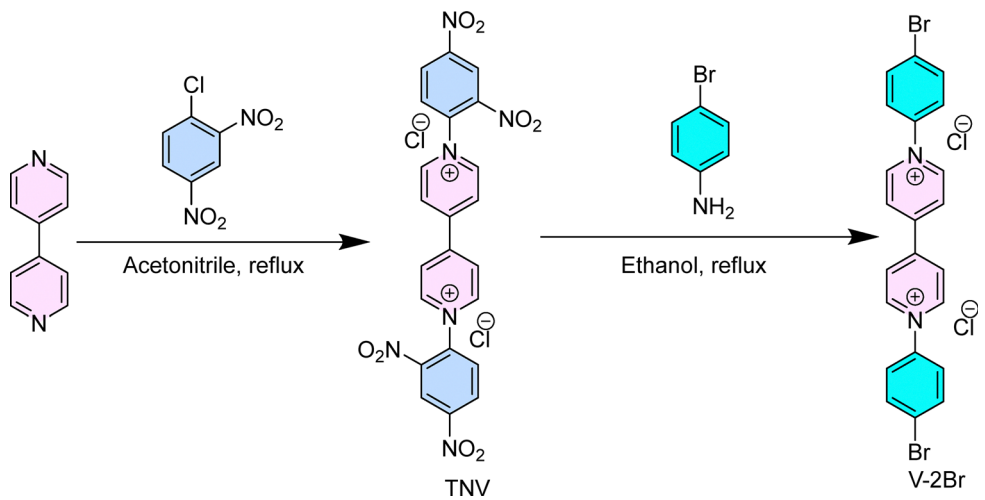

1′,1′-Bis(2,4-dinitrophenyl)-[4,4′-bipyridine]-1,1′-diium dichloride (TNV) was synthesized by refluxing 4,4′-bipyridine (4 g, 25.60 mmol) with 1-chloro-2,4-dinitrobenzene (26 g, 89.60 mmol) in 150 mL of anhydrous acetonitrile under an N_2 atmosphere for 72 hours. After the reaction was complete, the mixture was filtered, and the resulting solid was washed twice with acetonitrile (50 mL) and four times with diethyl ether (40 mL each) to remove the unreacted products. The solid was then recrystallized from diethyl ether, yielding pure TNV with a 75% yield. In a subsequent reaction, 1′,1′-bis(2,4-dinitrophenyl)-4,4′-bipyridine-1,1′-diium dichloride (0.500 g, 0.891 mmol) was combined with 4-bromoaniline (2.67 mmol) in ethanol and heated at reflux under nitrogen for 48 hours, resulting in a cloudy dark yellow reaction mixture. The progress of the reaction was monitored by TLC. The solvent volume was then reduced by evaporation, and the mixture was poured into rapidly stirring THF, forming a fine yellow precipitate. The precipitate was filtered, and the solid was washed with ether, yielding the final product (V-2Br) as a yellow solid.

4.3. Synthesis of the TAB[37–40]

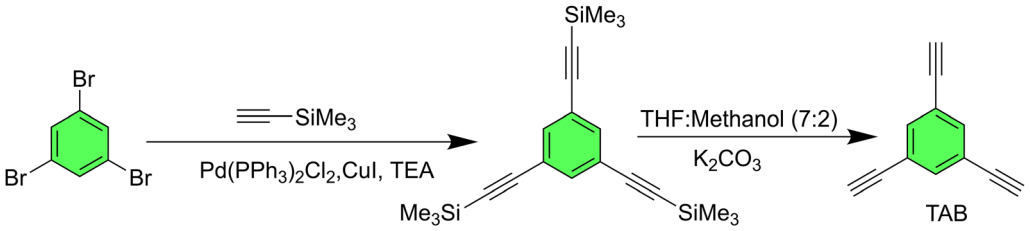

To a solution of commercially procured 1,3,5-tribromobenzene (503.0 mg, 1.59 mmol) in dry triethylamine (9.0 mL), $Pd(PPh_3)Cl_2$ (36.1 mg, 0.05 mmol) and CuI (10.0 mg, 0.05 mmol) were added, and the mixture was stirred under an argon atmosphere for 15 minutes. Trimethylsilylacetylene (0.9 mL, 6.33 mmol) was then added, and the reaction mixture was heated to 65 °C and stirred for 16 hours. After completion, hexane (25 mL) was added to the mixture, and it was subjected to short-path column chromatography on silica gel. The solvent was evaporated, and the residue was further purified by column chromatography on silica gel, eluting with hexane, yielding 1,3,5-tris(trimethylsilylethynyl)benzene as a pale yellow solid. This product was dissolved in tetrahydrofuran (7.0 mL) and methanol (2.0 mL). A solution of anhydrous potassium carbonate (26.9 mg in 0.4 mL of H_2O) was added, and the mixture was stirred at room temperature for 6 hours. Water (12 mL) was then added, and the organic solvents were evaporated. The residue was extracted with dichloromethane, washed with water and brine, and dried over anhydrous sodium sulfate, yielding 220.8 mg of TAB as an off-white solid.

4.4. Synthesis of the iVOF-2

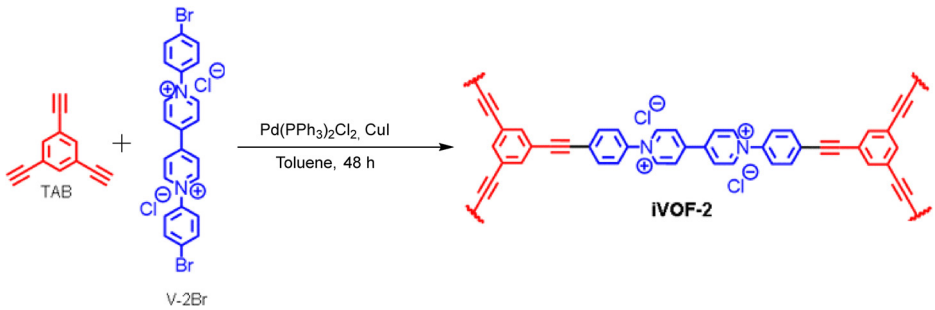

The synthesis of iVOF was performed following a previously reported procedure with slight modifications.[41] A 50 mL two-neck Schlenk flask was charged with 1,1′-bis(4-bromophenyl)-4,4′-bipyridinium chloride (V-2Br, 538 mg, 1.00 mmol) and 1,3,5-triethynylbenzene (TAB; 101 mg, 0.670 mmol) as monomers, along with CuI (5.71 mg, 30.0 μmol) and $Pd(PPh_3)_2Cl_2$ (15 mg) as catalysts. Dry toluene (20 mL) and triethylamine (10.0 mL) were subsequently injected into the reaction flask. The mixture was stirred at 110 °C for 48 hours, during which a brown powder gradually formed. After the reaction was complete, the mixture was cooled to room temperature. The precipitate was then collected by centrifugation, washed with methanol, and dried under vacuum.

4.5. Synthesis of the iVOF-2@MOF_Comp-1 to 3

For the preparation of iVOF-2@MOF_Comp-1, UiO-66-NH_2 (100 mg) was dispersed in a mixture of dry toluene (10 mL) and triethylamine (5 mL) in a 50 mL two-neck Schlenk flask. To this mixture, $(PPh_3)_2PdCl_2$ (1.7 mg, 2.4 μmol) and CuI (0.50 mg, 2.6 μmol) were added, and the resulting solution was stirred at 90 °C for 1 hour. Subsequently, TAB (10 mg, 0.066 mmol) and V-2Br (54 mg, 0.1 mmol) were introduced into the flask, and the reaction mixture was refluxed at 110 °C for 48 hours, during which a brown powder gradually formed. After completion, the reaction mixture was cooled to room temperature, and the precipitate (iVOF-2@MOF_Comp-1) was collected by centrifugation, washed with methanol, DCM, acetonitrile, THF and acetone, and dried under vacuum. For the preparation of iVOF-2@MOF_Comp-2, TAB (20 mg, 0.133 mmol) and V-2Br (108 mg, 0.2 mmol) were used, while for iVOF-2@MOF_Comp-3, TAB (30 mg, 0.2 mmol) and V-2Br (161 mg, 0.3 mmol) were added following the same procedure.

Data availability

All the additional data are available in the ESI.†

Conflicts of interest

The authors declare that there are no known conflicts of interest.

Acknowledgements

The authors thank the Indian Institute of Technology (IIT) Patna for financial support. A. Hassan and Sk A. Wahed thank IIT Patna for respective Institute Research Fellowships. The authors also acknowledge SAIF-IIT Patna for providing the NMR facilities.

References

1 T. Xue, T. He, L. Peng, O. A. Syzgantseva, R. Li, C. Liu, D. T. Sun, G. Xu, R. Qiu, Y. Wang, S. Yang, J. Li, J.-R. Li and W. L. Queen, *Sci. Adv.*, 2023, **9**, eadg4923.
2 J. N. S. Ang, A. Y. Chahine, T. J. Raeber, S. R. Batten and D. R. Turner, *Inorg. Chem.*, 2024, **63**, 1258–1265.
3 D. Mei and B. Yan, *Coord. Chem. Rev.*, 2025, **539**, 216769.
4 S. Abubakar, G. Das, T. Prakasam, A. Jrad, F. Gándara, S. Varghese, T. Delclos, M. A. Olson and A. Trabolsi, *ACS Appl. Mater. Interfaces*, 2024, **17**, 17794–17803.
5 Y. Chen, Q. Qiao, J. Cao, H. Li and Z. Bian, *Joule*, 2021, **5**, 3097–3115.
6 H. Shang, Y. Chen, S. Guan, Y. Wang, J. Cao, X. Wang, H. Li and Z. Bian, *Nat. Chem. Eng.*, 2024, **1**, 170–179.
7 F. Li, J. Zhu, P. Sun, M. Zhang, Z. Li, D. Xu, X. Gong, X. Zou, A. K. Geim, Y. Su and H.-M. Cheng, *Nat. Commun.*, 2022, **13**, 4472.
8 M. Peydayesh, E. Boschi, F. Donat and R. Mezzenga, *Adv. Mater.*, 2024, **36**, 2310642.
9 J. Cao, Z. Xu, Y. Chen, S. Li, Y. Jiang, L. Bai, H. Yu, H. Li and Z. Bian, *Angew. Chem., Int. Ed.*, 2023, **62**, e202302202.
10 X. Li, S. Chen, X. Hu and F. Zi, *Adv. Funct. Mater.*, 2024, **34**, 2307472.
11 M. Liu, D. Jiang, Y. Fu, G. Zheng Chen, S. Bi, X. Ding, J. He, B.-H. Han, Q. Xu and G. Zeng, *Angew. Chem., Int. Ed.*, 2024, **63**, e202317015.
12 A. Ding, M. Li, C. Liu, T.-S. Chee, Q. Yan, L. Lei and C. Xiao, *Sci. Adv.*, 2024, **10**, eadm9311.
13 M. R. Awual, M. A. Khaleque, M. Ferdows, A. M. S. Chowdhury and T. Yaita, *Microchem. J.*, 2013, **110**, 591–598.
14 H. Furukawa, K. E. Cordova, M. O'Keeffe and O. M. Yaghi, *Science*, 2013, **341**, 1230444.
15 H.-C. Zhou, J. R. Long and O. M. Yaghi, *Chem. Rev.*, 2012, **112**, 673–674.
16 Q.-L. Zhu and Q. Xu, *Chem. Soc. Rev.*, 2014, **43**, 5468–5512.
17 W. Guo, J. Liu, H. Tao, J. Meng, J. Yang, Q. Shuai, Y. Asakura, L. Huang and Y. Yamauchi, *Adv. Mater.*, 2024, **36**, 2405399.
18 A. Hassan, M. M. R. Mollah, S. Das and N. Das, *J. Mater. Chem. A*, 2023, **11**, 17226–17236.
19 T. Škorjanc, D. Shetty, M. A. Olson and A. Trabolsi, *ACS Appl. Mater. Interfaces*, 2019, **11**, 6705–6716.
20 S. Fajal, A. Hassan, W. Mandal, M. M. Shirolkar, S. Let, N. Das and S. K. Ghosh, *Angew. Chem., Int. Ed.*, 2023, **62**, e202214095.
21 J. Chun, S. Kang, N. Park, E. J. Park, X. Jin, K.-D. Kim, H. O. Seo, S. M. Lee, H. J. Kim, W. H. Kwon, Y.-K. Park, J. M. Kim, Y. D. Kim and S. U. Son, *J. Am. Chem. Soc.*, 2014, **136**, 6786–6789.
22 Y. Chen, Z. Li, R. Ding, T. Liu, H. Zhao and X. Zhang, *J. Hazard. Mater.*, 2022, **426**, 128073.
23 Q. Xu, X.-H. Du, D. Luo, M. Strømme, Q.-F. Zhang and C. Xu, *Chem. Eng. J.*, 2023, **458**, 141498.
24 J. Guo, X. Fan, J. Wang, S. Yu, M. Laipan, X. Ren, C. Zhang, L. Zhang and Y. Li, *Chem. Eng. J.*, 2021, **425**, 130588.
25 Y. Lei, Y. Xia, W. Chen, B. Lin, T. Li and L. Li, *Macromol. Rapid Commun.*, 2023, **44**, 2200712.
26 S. Abubakar, G. Das, T. Prakasam, A. Jrad, F. Gándara, S. Varghese, T. Delclos, M. A. Olson and A. Trabolsi, *ACS Appl. Mater. Interfaces*, 2025, **17**, 17794–17803.
27 R. Ding, Y. Chen, Y. Li, Y. Zhu, C. Song and X. Zhang, *ACS Appl. Mater. Interfaces*, 2022, **14**, 11803–11812.
28 D. T. Sun, N. Gasilova, S. Yang, E. Oveisi and W. L. Queen, *J. Am. Chem. Soc.*, 2018, **140**, 16697–16703.
29 T. Ma, R. Zhao, Z. Li, X. Jing, M. Faheem, J. Song, Y. Tian, X. Lv, Q. Shu and G. Zhu, *ACS Appl. Mater. Interfaces*, 2020, **12**, 30474–30482.
30 L. Zhang, Q.-Q. Zheng, S.-J. Xiao, J.-Q. Chen, W. Jiang, W.-R. Cui, G.-P. Yang, R.-P. Liang and J.-D. Qiu, *Chem. Eng. J.*, 2021, **426**, 131865.
31 Q. Ge and H. Liu, *Chem. Eng. J.*, 2023, **462**, 142323.
32 X. Li, Y.-L. Wang, J. Wen, L. Zheng, C. Qian, Z. Cheng, H. Zuo, M. Yu, J. Yuan, R. Li, W. Zhang and Y. Liao, *Nat. Commun.*, 2023, **14**, 263.
33 Y. Chen, M. Xu, J. Wen, Y. Wan, Q. Zhao, X. Cao, Y. Ding, Z. L. Wang, H. Li and Z. Bian, *Nat. Sustainability*, 2021, **4**, 618–626.
34 L. He, S. Liu, L. Chen, X. Dai, J. Li, M. Zhang, F. Ma, C. Zhang, Z. Yang, R. Zhou, Z. Chai and S. Wang, *Chem. Sci.*, 2019, **10**, 4293–4305.
35 T. Skorjanc, D. Shetty, S. K. Sharma, J. Raya, H. Traboulsi, D. S. Han, J. Lalla, R. Newlon, R. Jagannathan, S. Kirmizialtin, J.-C. Olsen and A. Trabolsi, *Chem. – Eur. J.*, 2018, **24**, 8648–8655.
36 A. Hassan, R. K. Pandey, A. Chakraborty, S. A. Wahed, T. R. Rao and N. Das, *Soft Matter*, 2024, **20**, 7832–7842.
37 M. I. Mangione, R. A. Spanevello and M. B. Anzardi, *RSC Adv.*, 2017, **7**, 47681–47688.
38 N. Baig, S. Shetty, S. Al-Mousawi and B. Alameddine, *Polym. Chem.*, 2021, **12**, 2282–2292.
39 N. Baig, S. Shetty, S. Al-Mousawi, F. Al-Sagheer and B. Alameddine, *Reactive Funct. Polym.*, 2019, **139**, 153–161.
40 B. Alameddine, N. Baig, S. Shetty, S. Al-Mousawi and F. Al-Sagheer, *Polymer*, 2018, **154**, 233–240.
41 H. Luo, S. Wang, X. Meng, G. Yuan, X. Song and Z. Liang, *Mater. Chem. Front.*, 2023, **7**, 2277–2285.